Available online at www.sciencedirect.com
SCIENCE DIRECT®
C. R. Physique 4 (2003) 1063–1074
COMPTES RENDUS PHYSIQUE

Carbon nanotubes: state of the art and applications/Les nanotubes de carbone : état de l'art et applications

Aspects of crystal growth within carbon nanotubes

Jeremy Sloan [a,b,*], Angus I. Kirkland [c], John L. Hutchison [b], Malcolm L.H. Green [a]

[a] *Inorganic Chemistry Laboratory, University of Oxford, South Parks Road, Oxford, OX1 3QR, UK*
[b] *Department of Materials, University of Oxford, Parks Road, Oxford, OX1 3PH, UK*
[c] *Department of Materials Science and Metallurgy, University of Cambridge, Pembroke Street, Cambridge CB2 3QZ, UK*

Presented by Guy Laval

Abstract

The comparative crystallisation and HRTEM imaging properties of simple binary halides formed by the alkali iodides MI (M = Li, K, Na, Rb and Cs) within single walled carbon nanotubes (SWNTs) are described. The most common structure type observed within SWNTs is the rocksalt archetype, although CsI was observed to form both *bcc* and rocksalt structure types. In SWNTs forming in the 1.2–1.6 nm diameter range, all of the incorporated halides showed preferred orientation, with the ⟨100⟩ growth direction predominating for rocksalt-type packing and ⟨112⟩ so far observed exclusively for *bcc* packing. Crystals with dimensions spanning 2–6 atomic layers thickness in projection invariably exhibited lattice expansions that were attributed predominantly to a net reduction in coordination at the crystal-carbon interface. The crystallisation behaviour of UCl_4–KCl and AgI–AgCl eutectic melts was compared in carbon nanotubes of different diameters and a pronounced ordering influence over the normally glassy melts was observed in narrower capillaries. HgI_2 crystallised within nanotubes with ultra-narrow (i.e., 0.8 nm) capillaries were observed to form helical 2×1 layer crystals. ***To cite this article: J. Sloan et al., C. R. Physique 4 (2003).***

Résumé

Cristallisation à l'intérieur de nanotubes de carbone. Cette étude décrit la cristallisation et l'imagerie HRTEM d'hallogènes binaires simples formés de iodures alcalins MI (M = Li, K, Na, Rb, et Cs) à l'intérieur de nanotubes de carbone à paroi unique (SWNT). Bien que le type de structure habituellement observée à l'intérieur des SWNT soit de type NaCl, CsI semble former des structures *cc* ainsi que des structures de type NaCl. Pour les SWNT de l'ordre de 1,2 à 1,6 nm de diamètre, tous les types d'hallogènes adoptent une orientation privilégiée, avec une direction de croissance ⟨100⟩ dominante pour le type d'arrangement NaCl, et ⟨112⟩ obtenu exclusivement dans le cas des arrangements de type *cc*. Les cristaux d'épaisseur comprise entre 2 et 6 couches d'atomes produisent invariablement des dilatations de réseau principalement attribuées à une réduction nette de coordination à l'interface cristal-carbone. La cristallisation de liquides eutectiques de UCl_4–KCl et de AgI–AgCl a été étudiée pour des nanotubes de carbone de différents diamètres et une tendance prononcée à la mise en ordre cristalline préférentiellement à l'état vitreux a été observée dans les capillaires les plus fins. HgI_2 cristallise dans des nanotubes capillaires ultrafins (ex : 0,8 nm) en formant des couches cristallines helicoïdales 2×1. ***Pour citer cet article : J. Sloan et al., C. R. Physique 4 (2003).***

1. Introduction

Carbon nanotubes, in particular, single walled carbon nanotubes (SWNTs) [1,2] have shown themselves to be ideal model systems for templating atomically regulated 1D crystal growth [3]. These nm scale tubules are composed of individual rolled

* Corresponding author.
E-mail addresses: jeremy.sloan@chem.ox.ac.uk (J. Sloan), aik10@cus.cam.ac.uk (A.I. Kirkland), john.hutchison@materials.ox.ac.uk (J.L. Hutchison), malcolm.green@chem.ox.ac.uk (M.L.H. Green).

1631-0705/$ – see front matter
doi:10.1016/S1631-0705(03)00102-6

sheets of sp^2 graphene carbon and form well-defined cylindrical cavities within a strictly limited diameter range (typically 1–2 nm) when prepared, for example, by Krätschmer–Huffman synthesis [4], laser ablation [5] or catalytic decomposition of carbon monoxide [6]. The effect of the size of these ultra-thin capillaries on the crystallisation of molten ionic compounds has been to produce 1D crystals that are systematically reduced in coordination and which display structural distortions relative to the parent bulk structure [3,7–10]. The extent to which a particular structure is modified by incorporation has been shown to be a function of both the relative complexity of the material being incorporated, the confining geometry of the nanotube and its morphology [3,7–13]. In the case of simple packed structures, crystals with integral numbers of atomic layers can be produced as a function of the nanotube diameter [3]. For more complex crystal structures, capillary confinement can result in the formation of 1D-polyhedral chains or structures with entirely novel co-ordinations and stereochemistry [9,10]. Such observations are of fundamental importance because of what they tell us about materials restricted to the smallest conceivable dimensions. The ultimate goal of nanotechnology will be to synthesize devices from materials formed on such a scale and it will only be possible to understand the true physical nature of such materials if they can be fully studied on both an ab initio and experimental basis.

Currently, the best experimental methodology for studying the composite structure of nanotube encapsulates is direct or indirect atomic resolution electron imaging techniques performed in a high resolution transmission electron microscope (HRTEM) [14]. These techniques are favoured as they are capable of imaging the nanocomposites in a 2D projection with the result that information from both the nanotube and the encapsulated material can be made available [15]. Although it has been shown recently that scanning tunnelling microscopy (STM) can also detect fullerene and endofullerene encapsulates inserted into SWNTs, the detailed structures of these encapsulates is indistinct as their structures are blurred by the nanotube walls although local band structure modulations of the tubules can be detected [16,17]. As SWNT and other nanotube encapsulates approach ideal weak phase objects then electron imaging techniques can be used optimally without the usual concerns over specimen thickness. In addition, further cues regarding the thickness of nanotube encapsulates species can be inferred from the symmetry of the cylindrical nanotubes [14]. As with STM, in situ spectroscopic techniques including energy dispersive microanalysis (EDX) and electron energy loss spectroscopy (EELS) can provide additional chemical information concerning the specimens.

Recently, the crystal growth behaviour of molten species in SWNTs has been investigated theoretically via molecular dynamics simulations [11–13]. While these investigations have been mostly confined to a single binary halide (i.e., KI), they have revealed some valuable information concerning possible mechanisms of crystal growth inside carbon nanotubes, in addition to duplicating some of the experimentally observed structural distortions [7,8] and predicting other structural behaviour, including 1D crystal 'twisting' and crystal growth behaviour in partially and fully uncapped nanotubes. In this laboratory the crystallisation behaviour of a wide variety of binary and ternary halides has been studied according to bulk structure type and respective imaging behaviour of the constituent ions [3,14,18,19]. In this article we will review some of the experimental aspects of observed crystal growth behaviour in carbon nanotubes, both in attempt to address some of the theoretical issues that have been raised and also by way of introducing some as-yet unforeseen crystal growth phenomena. We will also discuss *in tandem* issues pertinent to the imaging behaviour and interpretation of these 1D crystal systems.

2. Comparative crystal growth behaviour of alkali metal iodides in single-walled carbon nanotubes

One of the more remarkable features of the crystal growth behaviour of simple packed structures in single walled carbon nanotubes is that the obtained 1D crystals are atomically regulated in cross section by the diameters of the confining tubules, as mentioned in the introduction [3,7,8,14]. Such a consideration raises the prospect that, providing that 'single phase' nanotubes (i.e., tubules of pure, unique (n, m) conformation and diameter) can be produced, then bulk samples of nanotubes containing crystals with precise integral atomic layer architectures can be produced, assuming quantitative filling.[1] Another important assumption is that the filling materials always crystallize in a predictable way according to SWNT diameter.

Previously, we have shown that KI forms effectively $2 \times 2 \times \infty$ and $3 \times 3 \times \infty$ 1D crystals inside SWNTs of diameters 1.4 nm and 1.6 nm, respectively [7,8]. These crystals were formed in preferred orientation with $\langle 001 \rangle$ relative to the rocksalt form of the halide obtained parallel to the tubule axes. In the case of the $3 \times 3 \times \infty$ crystals a modified HRTEM image restoration approach made possible an atom-by-atom interpretation of the crystallography of the incorporated crystal [8]. The two layer crystal was imaged by conventional HRTEM and the lattice images showed a tetragonally distorted crystal consisting of an alternating arrangement of K–I and I–K columns with a total reduction in co-ordination reduced from 6 : 6 (i.e., bulk KI) to 4 : 4, occurring as a result of SWNT confinement. For the $3 \times 3 \times \infty$ crystal, a systematic reduction of the face and edge …I–K–I–K… atom rows arranged parallel to the SWNT axis is produced while the central …I–K–I–K… rows retain the bulk coordination [8].

[1] High-yield and near-quantitative filling has already been demonstrated for fullerene molecules incorporated into SWNTs [20,21] whereas 70% filling of SWNTs has been demonstrated for certain halides [22].

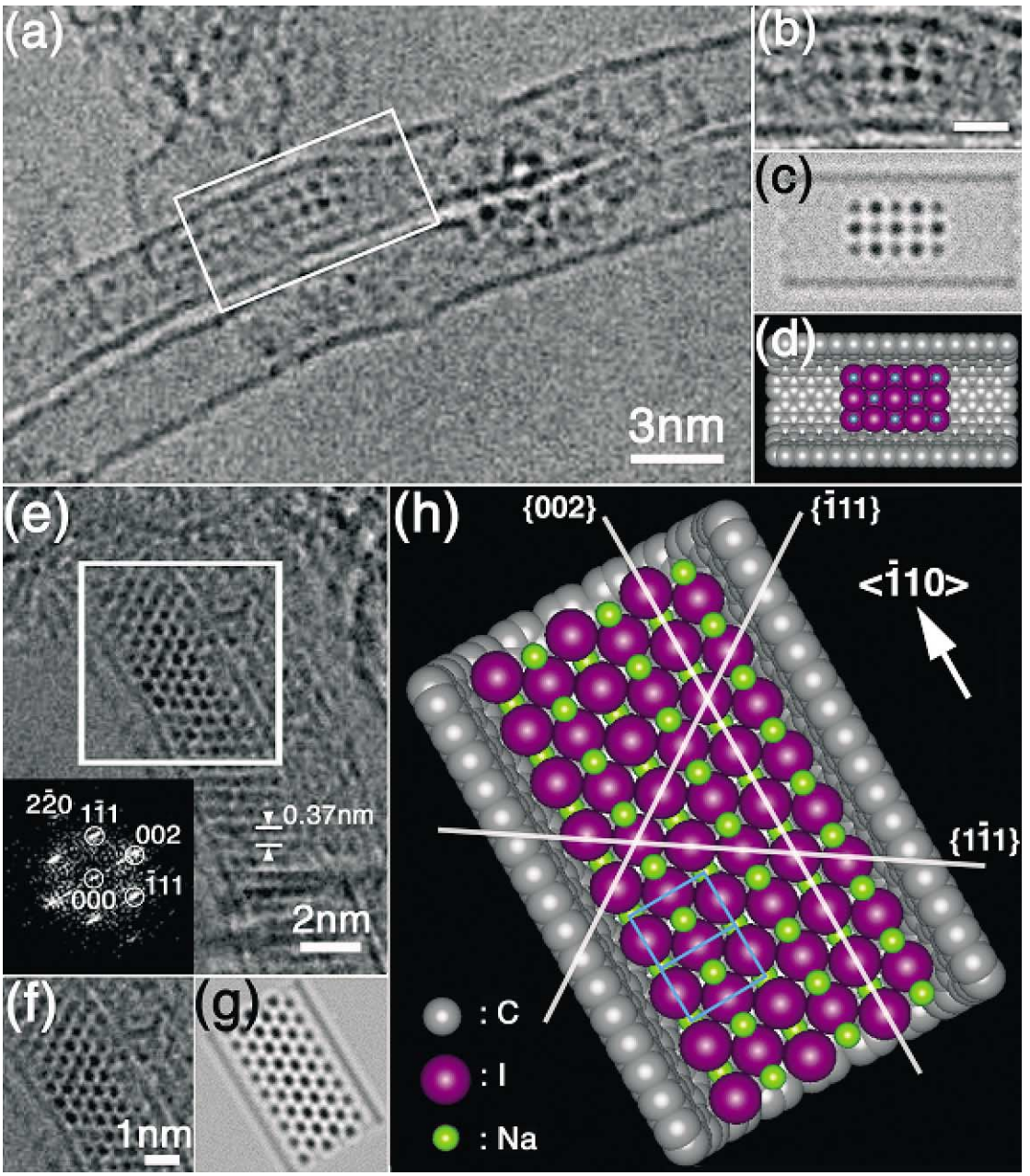

Fig. 1. (a) HRTEM lattice image of a pair of SWNTs, one of which contains a $3 \times 3 \times 5$ cluster of LiI viewed along $\langle 001 \rangle$. (b) Enlargement of boxed region in (a). Image contrast is wholly due to the strongly scattering I^- species. (c) and (d) Scherzer focus HRTEM image simulation and corresponding structure model of $3 \times 3 \times 5$ cluster (purple spheres $= I^-$; blue spheres $= Li^+$). (e) $\langle 110 \rangle$ projection lattice image and corresponding power spectrum (inset) of a 6-layer thick NaI 1D crystal formed in a wide diameter SWNT. Note that, in the lower part if the image, the bend in the crystal caused by the SWNT curvature or, alternatively, a tilt in the SWNT angle causes only the lattice planes arbitrarily assigned $\{-111\}$ to be visible (indicated). (f)–(h) Detail from lattice image, Scherzer focus image simulation and corresponding structure model with lattice planes and growth direction indicated. All the atom columns in this orientation are 'pure' atom columns but, due to the low scattering power of Na^+, only the I^- columns are visible.

These and other crystal fillings were obtained, except where otherwise stated, by mixing SWNTs prepared via an arc synthesis procedure by mixing the molten halide with the as-prepared tubules according to an established procedure [23–25]. In addition to the KI system, we have investigated the crystal growth behaviour of the other alkali iodides (i.e., MI, M = Li, Na, Rb and Cs) in this system. Of particular interest was the comparative imaging properties of the M^+ ion as a function of scattering power and the lattice distortions of these crystals relative to the bulk structures of the respective filling material. The iodides were deemed to be ideal for this purpose as all the halides within the homologous series would be visible via HRTEM due to the strong scattering power of I^- whereas the extent of visibility of the counter-ions would be determined by their respective scattering power relative to I^-. Figs. 1(a)–(d) shows, for example, the formation of LiI in a bundle consisting of two 1.6 nm diameter SWNTs imaged in a 300 kV field emission gun HRTEM (i.e., JEOL 3000F, $C_S = 0.57$ mm). This filling only appears fleetingly at the employed magnification as it was very beam sensitive. As a result, in this image we only see a small $3 \times 3 \times 5$ rocksalt cluster viewed, in this case, along ⟨001⟩. The rest of the filling in the micrograph has been rendered glassy by the electron beam. We assume that the dark spots in the cluster are due to either I–Li–I or Li–I–Li columns viewed parallel to the electron beam. A further remarkable feature concerning this cluster is that it expanded considerably relative to the bulk form of the halide. The average {200} lattice spacing measured parallel to the SWNT axis is 0.37 nm, whereas measured orthogonal to the axis, this spacing is 0.36 nm, which compares to a calculated value of 0.2965 nm based on the published structure (see Table 1 [26–29]). If correct, this represents a lattice expansion of nearly 25% both along and across the capillary. Previously, we have reported a lattice expansion of 14% for $2 \times 2 \times \infty$ KI formed within a 1.4 nm diameter SWNT, an expansion subsequently duplicated by molecular dynamics simulations [11,12]. With respect to the encapsulated LiI cluster viewed in Fig. 1(a), the situation is complicated by the fact that the crystal was found to rearrange in the beam after only a few seconds and we therefore do not know if this expansion is 'real' or beam-induced (see for example Ref. [30]). Crystals of NaI formed within SWNTs were generally more robust in the electron beam than LiI and longer continuous crystalline filling was observed inside many capillaries. In the example in Figs. 1(e)–(h), a six layer crystal is shown formed inside a 2.5 nm diameter SWNT. This crystal is imaged with ⟨110⟩ parallel to the electron beam and with a growth direction of $\langle \bar{1}10 \rangle$ projecting along the capillary. In this projection, as for the previously imaged $3 \times 3 \times \infty$ KI crystal formed in a 1.6 nm diameter SWNT [8], all the atom columns image as pure atom columns and thus the 0.37 nm spaced rows of dark spots visible in Figs. 1(e) and (f) corresponding to rows of I^- columns arranged at 55° to the SWNT walls. The pure Na^+ columns, which reside in the columns of octahedral interstices formed between the I^- columns, are effectively invisible due to their weak scattering power. This can be verified by comparing the detail in Fig. 1(f) to the Scherzer focus simulation shown in Fig. 1(g) and the structure model in Fig. 1(h). From this new projection, we can identify similar lattice distortions to those reported for the KI fillings [7,8]. The {200} planes, which are arranged parallel to the SWNT axis (cf. Figs. 1(f) and (h)), are spaced at 0.337 nm intervals across the capillary which represents

Table 1
Measured d-spacings of alkali iodides obtained from HRTEM lattice images. The estimated precision in all measurements is ±0.02 nm

Halide filling	Figure No.	Bulk structure type	Corresponding bulk *hkl* lattice plane	Measured w.r.t. SWNT axis	Measured d-spacing (nm)	Corresponding literature *hkl* d-spacing (nm)[1]
LiI	Fig.1(a)	Rocksalt	200	Longitudinally	0.37	0.2965 [26]
"	"	"	"	Across	0.36	"
NaI	Fig. 1(e)/(f)	Rocksalt	200	Longitudinally	0.34	0.324 [27]
"	"	"	111	Diagonally	0.37	0.374 [27]
KI	Fig. 2(a)	Rocksalt	200	Longitudinal	0.35	0.352 [28]
"	"	"	"	Across	0.37	"
KI	Fig. 2(f)	Rocksalt	200	Longitudinal	0.37	0.352 [28]
"	"	"	"	Across	0.38	"
RbI	No figure	Rocksalt	200	Longitudinal	0.36	0.3665 [28]
"	"	"	"	Across	0.39	"
CsI	Fig. 3(a)	*bcc*	−110	Diagonally	0.35	0.3196 [26]
"	"	"	01−1	"	0.32	"
"	"	"	10−1	"	0.32	"
CsI	Fig. 3(f), (g)	*bcc*	−110	Diagonally	0.33	0.3196 [26]
"	"	"	−101	"	0.35	"
"	"	"	01−1	"	0.34	"
CsI (2 ×2)	Fig. 3(j)	Rocksalt	200	Longitudinal	0.37	0.381 [29]
"	"	"	"	Across	0.41	"
CsI (3 ×3)	Fig. 3(m)	Rocksalt	200	Longitudinal	0.39	0.381 [29]
"	"	"	"	Across	0.42	"

[1] Calculated from published crystal structures.

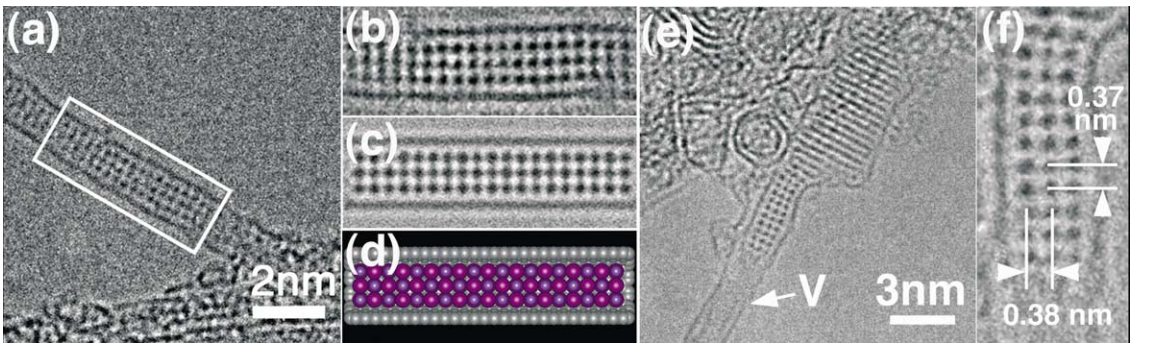

Fig. 2. (a) HRTEM image of a $3 \times 3 \times \infty$ 1D KI crystal viewed along ⟨001⟩ with respect to the bulk phase. (b)–(d) Detail from boxed region in (a), Scherzer focus image simulation and corresponding structure model of $3 \times 3 \times \infty$ crystal (purple spheres = I^-; red spheres = K^+). (e) Variable diameter KI crystal in an asymmetric funnel-shaped SWNT which terminates in the narrower section, resulting in an empty region (indicated **V**). Either side of the constriction the 1D crystal is twisted in such a way that the ⟨001⟩ projection is visible only in the narrower section of SWNT. In the wider section of the SWNT, the {100} lattice planes are visible in an orientation orthogonal to the SWNT axis. (f) Detail from (e) showing the distances between the {100} lattice planes organized parallel to the SWNT axis and the {010} lattice planes orientated orthogonally with respect to the SWNT axis.

a 4% expansion relative to the bulk phase. By contrast, the {111} lattice planes, measured diagonally across the capillary, are slightly contracted (see Table 1). These are smaller lattice distortions than those reported for $2 \times 2 \times \infty$ and $3 \times 3 \times \infty$ KI [7,8], but this is perhaps to be expected as the crystal is more 'bulk'-like as it contains more atomic layers in cross section.

In Figs. 2(a)–(d), we see a further example of a $3 \times 3 \times \infty$ KI crystal formed within a 1.6 nm diameter SWNT. This time, the crystal is imaged along ⟨001⟩ with respect to the bulk phase whereas the previously reported version was imaged along ⟨110⟩ [8]. The averaged lattice spacings of the {200} layers measured longitudinally with respect to the SWNT axis in this case correspond to 0.35 nm. For the crystal imaged along ⟨110⟩, we reported a similar spacing of 0.348 nm which is slightly contracted from the value calculated from the literature crystal structure (Table 1). In Fig. 2 (e) and (f), a KI crystal with a growth direction is seen to rotate about the SWNT axis either side of an expansion in the encapsulating SWNT. Of the other alkali iodides that we have studied, only $3 \times 3 \times \infty$ RbI [22] undergoes a similar contraction (see Table 1). Across the capillary, the {020} layers in Fig. 1 (a) and (b) expand from 0.35 nm to 0.37 nm, which is consistent with the d-spacings of {010} layers recorded differentially from K2I3K2IK slabs (i.e., 0.369 nm)[2] of the $3 \times 3 \times \infty$ KI fragment imaged along ⟨110⟩ although not so well with similar spacings recorded from I2K3I2KI slabs (i.e., 0.35 nm) [8]. The latter slabs are believed to be compressed due to the large size of the I^- ions and the compressing influence of the nanotube walls [8,11]. In addition to imaging the $3 \times 3 \times \infty$ KI crystal along ⟨001⟩, we have also imaged RbI crystallites in a similar projection [22]. Along the capillary, the {100} layers showed virtually no expansion but, across the capillary, the {010} layers were expanded slightly from 0.3665 nm to 0.37 nm across the capillaries (Table 1).

For all of the iodides from Li to Rb, the predominant structure type observed by HRTEM inside SWNT capillaries has been the rocksalt form. For LiI and NaI, this should be an anticipated result, as their respective $M^+ : I^-$ radius ratios of 0.437 and 0.563 favour octahedral coordination which is predicted in the range 0.414–0.592 [31]. The halides KI, RbI and CsI, have radius ratios of 0.738, 0.806 and 0.877, respectively, and these are all above the minimum radius ratio of 0.732 for which *bcc* 12-coordination is anticipated [31]. Experimentally, we have observed that only CsI forms significant quantities of *bcc*-type halide in SWNT capillaries. In Figs. 3(a)–(f), two examples of *bcc*-type CsI imaged in wide and narrow SWNT capillaries are presented, respectively. In both examples, the growth direction is effectively ⟨11−2⟩ and the inter-columnar distances and corresponding lattice spacings are consistent with the bulk form of *bcc* CsI [26], taking into account the small observed lattice distortions (Table 1). We only observed this projection in about 20% of all the observed crystals – all of the other crystals exhibited similar crystal growth behaviour to the other iodides in this series, as described above. In the case of the larger crystal (i.e., Fig. 3(a), indicated region II) there is clearly some variation in the crystal thickness, as evidenced by the variation of the atom column contrast out from the centre of the crystal. This may be caused either by facetting or by the crystal taking on a more cylindrical shape in cross-section. The extent to which either of these phenomena occur is difficult to verify from single HRTEM images although this phenomena is the subject of further investigations in this laboratory. In Figs. 3(j)–(o) we see the

[2] Note that these lattice spacings were estimated by multiplying the summed measured distances reported for the K and 2I layers and the 2I and 3K layers by $\sqrt{2}$ [8]. For these lower resolution HRTEM images, we were not able to observe differential expansions of the K2I3K2IK layers versus the I2K3I2KI layers but instead here report average layer distortions.

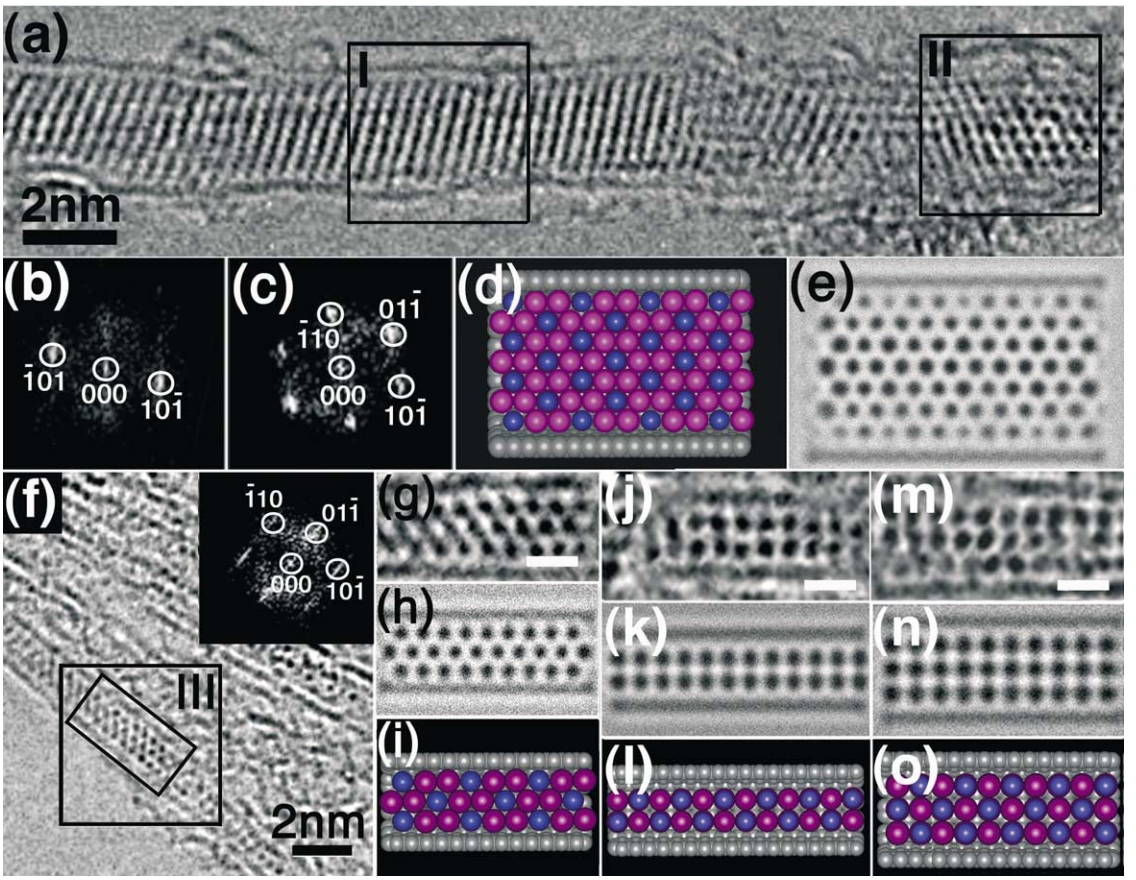

Fig. 3. (a) HRTEM lattice image of a long, wide bore SWNT filled with CsI (*bcc* form). (b) and (c) power spectra obtained from regions **I** and **II** in (a). (d) and (e) cutaway structure model and corresponding Scherzer image of *bcc* CsI crystal in ⟨111⟩ projection relative to the bulk phase. The image was calculated assuming the crystal to be 3 atom layers thick at the SWNT walls and 7 atoms thick in the centre. (f) HRTEM image showing a narrow (∼1.4 nm diameter) SWNT filled with *bcc* CsI, growth direction ⟨110⟩. Inset power spectrum **III** indicates that this crystal is viewed in ⟨111⟩ (cf. (a)II and (c)). (g)–(h) Detail (scale bar = 1 nm), Scherzer focus simulation and corresponding structure model of three layer thick CsI fragment. (j)-(l) HRTEM image (scale bar = 1 nm), Scherzer focus simulation and corresponding structure model of a $2 \times 2 \times \infty$ rocksalt CsI fragment in a 1.4 nm diameter SWNT. (m)–(o) as for (j)–(l) but for a $3 \times 3 \times \infty$ rocksalt CsI fragment in a 1.6 nm diameter SWNT (all models, purple spheres I^-, blue spheres = Cs^+).

more usual (i.e., for this halide) $2 \times 2 \times \infty$ and $3 \times 3 \times \infty$ rocksalt-type CsI crystals formed in 1.4 nm and 1.6 nm diameter SWNTs, respectively.

We believe that this phenomenon of preferred structure type and preferred orientation within narrow carbon capillaries is essentially stoichiometry-driven. Whenever we observe the rocksalt type structure, the growth direction is almost always parallel to the ⟨100⟩ direction, except in a few instances where the observed growth direction is equivalent to ⟨110⟩ (e.g., Figs. 1(e)–(h)). For both growth directions, the crystal is allowed to form along the narrow SWNT capillaries and terminate against their walls in such a way that the obtained crystal maintains a strict 1 : 1 anion/cation ratio, which can be verified by inspection (see Figs. 1(d), 1(h) and 1(d)). For example, a 1D crystal of repeating individual unit cells of KI growing parallel to ⟨100⟩ along a 1.6 nm SWNT capillary (i.e., a $3 \times 3 \times \infty$) is entirely stoichiometric as, along the capillary, it forms a bimodal array of complimentary K–2I–3K–2I–K and I–2K–3I–2K–I layers [8]. Similarly, a $2 \times 2 \times \infty$ KI crystal formed along a 1.4 nm capillary forms a 1D crystal with a stoichiometric ratio of K–2I–K and I–2K–I layers. A single unit cell of *bcc* CsI projecting along [100] inside a SWNT with a diameter into which it will snugly fit (ca. 0.8–1 nm) will have an anion/cation ratio of 4 : 1, by inspection. Logically, only a small number of growth directions are permissible for this structure type within a narrow capillary carbon nanotube. In the two examples in Figs. 3(d)–(f) and (g)–(i), the preferred growth direction is parallel to ⟨112⟩ and, if we add the corresponding top and bottom layers to the cutaway models shown in Fig. 3 (d) and (i), we can produce a stoichiometric 1D crystal. Aside from these, which we have observed experimentally, only a few other crystal growth directions could possibly be countenanced for this structure type (e.g., ⟨110⟩).

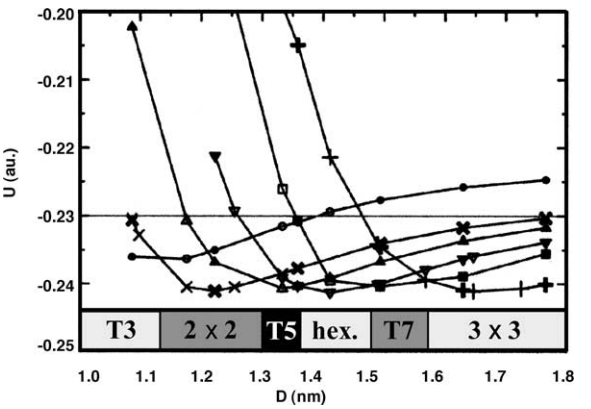

Fig. 4. Minimum energy (U) phase diagram depicted for structure types of KI predicted to fill SWNTs of varying diameter (D). T3, T5 and T7 are helical KI 1D crystals with 3, 5 and 7 membered rings in cross section, respectively (adapted from [13]).

It is interesting to note that the above experimental observations appear to be borne out by theoretical considerations, at least for the KI system. The crystal growth behaviour of KI in nanotubes with diameters in the range 1–1.8 nm have been calculated by molecular dynamics simulations [11–13]. In these calculations, rigid (n, m) SWNTs of differing diameters, in which the C atoms in were described by Lennard–Jones potentials, were immersed in 'molten' K^+ and I^- ions defined in terms Born–Mayer potentials and the composites allowed to attain a minimum energy configuration. As a result, a phase diagram (Fig. 4) could be constructed which predicts, in an *ab initio* fashion, the predominant structure type for the typical median range of nanotube diameters which form for SWNTs formed by catalytic arc synthesis [13,23]. For diameter ranges of 1.1–1.3 nm and 1.6–1.8 nm, effectively $2 \times 2 \times \infty$ and $3 \times 3 \times \infty$ rocksalt-type 1D KI crystal structures are predicted. Outside these ranges, other 1D crystal structures are expected. In the lowest diameter range studied (i.e., 1.0–1.1 nm), a so-called T3 structure is predicted, which is a twisted crystal structure in which the cross-section of the crystal consists of a three-membered ring (i.e., –I–K–K– or –I–I–K–). Similarly, in the ranges 1.3–1.35 nm and 1.47–1.55 nm, T5 and T7 twisted 1D crystal structures with 5– (e.g., –I–K–I–K–I–, etc.) and 7– (e.g., –I–K–I–K–I–K–I–, etc.) membered rings formed in cross section, respectively. In one range, from 1.35–1.47 nm, a so-called 'hex.' structure is formed in which the encapuslated structure can best be described in terms of a stacked 1D array of alternating 6-membered shells of the form –I–K–I–K–I–K- and –K–I–K–I–K–I–. In spite of the fact that KI just fulfils the radius ratio criterion for the formation of the *bcc* form (see above), which in fact does form under conditions of high pressure [32], this structural form was not one of the structure types predicted to form in this study.

3. Unusual structural growth behaviour encountered in narrow capillary carbon nanotubes

3.1. Nanotube induced variations in local 1D crystal structure

Although most of the 1D crystals that we have observed maintain a consistent local structure longitudinally over the distance of the imaged nanotube (typically 10–100 nm), this is not always the case. Defects in the nanotubes or, alternatively, induced stresses such as bending can cause considerable local variations in the crystal growth behaviour or block it entirely as we observed for a 1D crystal of $ThCl_4$ formed within a bent SWNT [3]. In addition, blockages within SWNTs can impede crystal growth behaviour as in, for example, the incorporation of fullerene molecules within SWNTs which can block 1D crystal growth in SWNTs [33,34].

Occasionally, side wall defects can affect crystal growth behaviour in SWNTs. In Fig. 2(e), we see a rather extreme example in which such a combination of such defects has lead to widening of the SWNT and a corresponding widening of the included crystal, in this case rocksalt KI. This has lead to the formation of an asymmetric funnel-shaped SWNT in which the narrower region corresponds to a 1.6 nm nanotube and forms a short section of 3×3 KI crystal which terminates after $\sim$10 {100} layers and a wide section about 3.8 nm in diameter. The crystal is found to be rotated either side of the nanotube junction with the result that, in the narrower section, the I–K–I and K–I–K columns are clearly visible, as in a ⟨001⟩ projection (cf. Figs. 2(a)–(d)), whereas in the wider section, lattice fringes corresponding to the {100} layers only are visible. Another interesting feature of this crystallite is that in the short, narrow section, we see a small expansion in both the {100} and {010} layers to 0.37 nm and 0.38 nm, respectively. These effects are possibly due to the crystal being formed in a slightly wider SWNT and also due to the termination of the crystal which will result in a systematic lowering of coordination at the termination surface thus resulting in a local relaxation of the crystal.

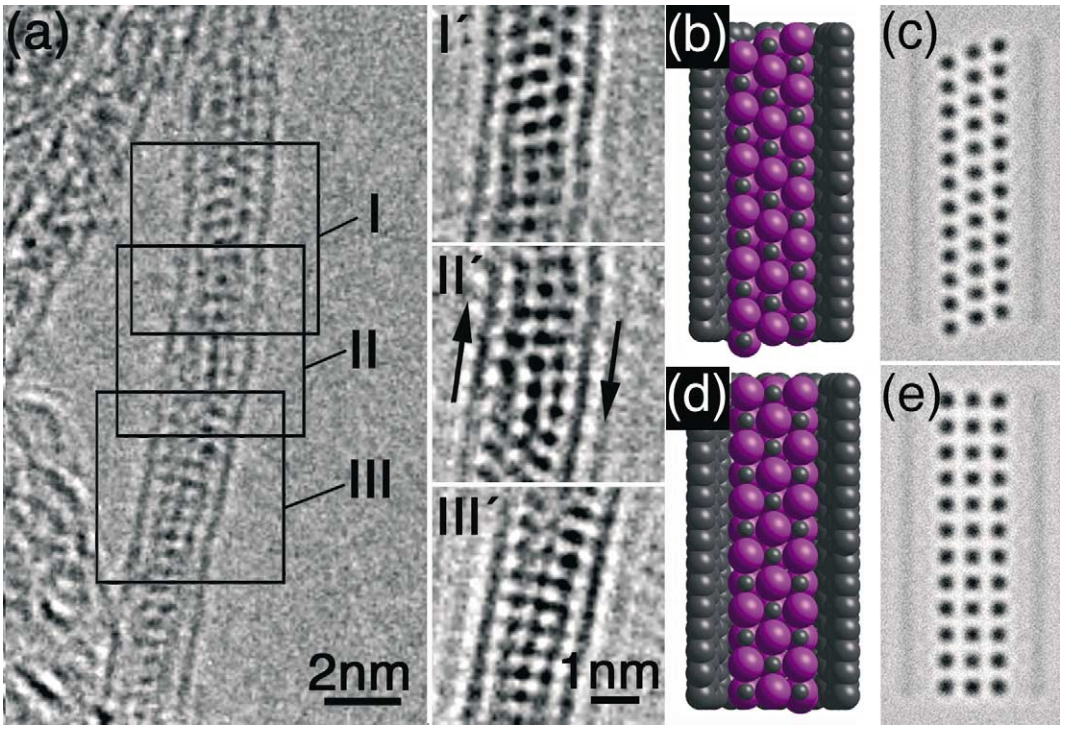

Fig. 5. (a) HRTEM image of an individual 1.6 nm diameter SWNT filled with pure AgI. **I′**, **II′** and **III′** show noise-filtered regions corresponding to regions **I**–**III** in the main image. Note how the sheared form (**I′**) transforms, via an intermediary region (**II′**) to a rocksalt like region (**III**). (b) and (c) model and simulation derived from packing observed in **I′**, (d) and (e) model and simulation derived from packing observed in **III′** (all models, purple spheres I^-, black spheres $= Ag^+$).

A second type of SWNT-induced distortion is shown in Figs. 5(a)–(e). The main micrograph (Fig. 5(a)) shows a ∼20 nm long section of a 1.6 nm diameter SWNT which is completely filled with AgI. In the lower part of the micrograph, this SWNT is straight although at the top of the micrograph, it is displaced by about 1 nm by a progressive bend along the nanotube length. Close inspection of three sub-regions of this micrograph (i.e., **I**, **II** and **III**) show clearly that, either side of the bend, the microstructure has altered from a sheared form (i.e., **I′** and Fig. 5 (b) and (c)) to a non-sheared, rocksalt form (i.e., **III′** and Fig. 5 (d) and (e)). In between is an intermediate region between the two section of crystal (i.e., **II′**). If we consider the central Ag {010} layer in the crystal (i.e., as viewed in **I′**, **II′** and **III′**) as being 'stationary' then the observed shear is considerable as it involves displacing the two outermost {010} layers by approximately one-half of the separation between the normal separation between {100} AgI layers (i.e., for the F*m*3*m* form, 0.152 nm [35]).

3.2. Influence of nanotube diameter on crystal growth behaviour of eutectic melting systems

While we have not been able to confirm or disprove the formation of shell-like binary crystals of the form predicted by Wilson [13], we have observed shell-like 1D crystal structures in the ternary KCl–UCl_4 systems and for the AgI:AgCl system formed in narrow capillary MWNTs and SWNTs [36,37]. In both instances, the compositions introduced corresponded to eutectic melting compositions in the respective phase diagrams (i.e., Fig. 6 (a) and (b)) and not to a binary composition.

For the KCl–UCl_4 system, we have observed the crystal growth behaviour of two eutectic compositions (i.e., compositions A and B, corresponding to 73.2 mol%KCl : 26.8 mol%UCl_4 and 50 mol%KCl : 50 mol%UCl_4, respectively). HRTEM images from composition B are reproduced here (Fig. 7 (a) and (b)) [36]. In this case, a glassy or polycrystalline filling forms in the wide ∼4 nm diameter MWNT (Fig. 7(a)) whereas a much more periodic crystalline filling is observed to form in the narrower ∼1 nm diameter MWNT capillary (Fig. 7(b)). It is interesting to note that this filling is most crystalline along the walls of the capillary, forming well defined rows of dark spots along them which we attribute to UCl_x polyhedra. Between these rows, the microstructure is less well defined. Similar results were observed for the second composition (i.e., composition A, Fig. 6(a)).

More recently, we have been able to observed the crystallisation of similar eutectic compositions within SWNTs [25, 37]. EELS linescans obtained in a scanning transmission electron microscope (STEM) confirmed that all three elements corresponding to the eutectic composition of the AgI–AgCl system were present in SWNTs filled with this mixture (see

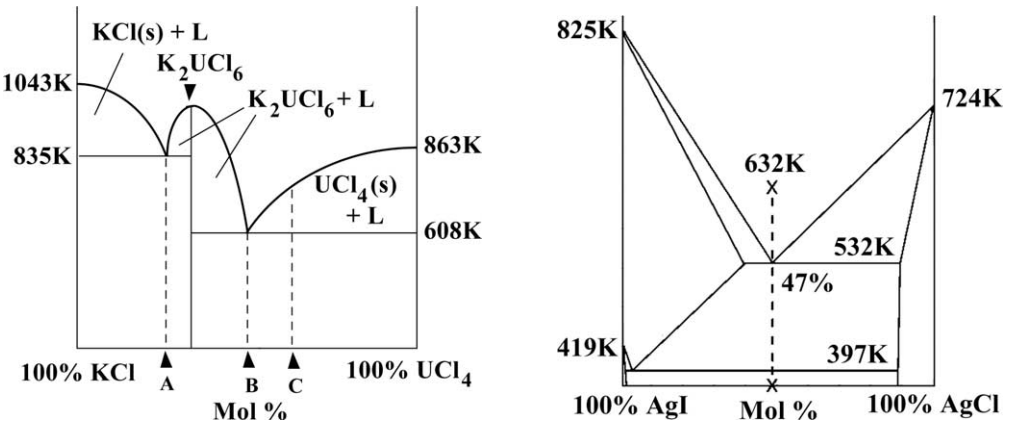

Fig. 6. (a) Schematic depiction of the KCl–UCl_4 pseudoternary phase diagram. (b) Schematic depiction of the AgI–AgCl pseudoternary phase diagram.

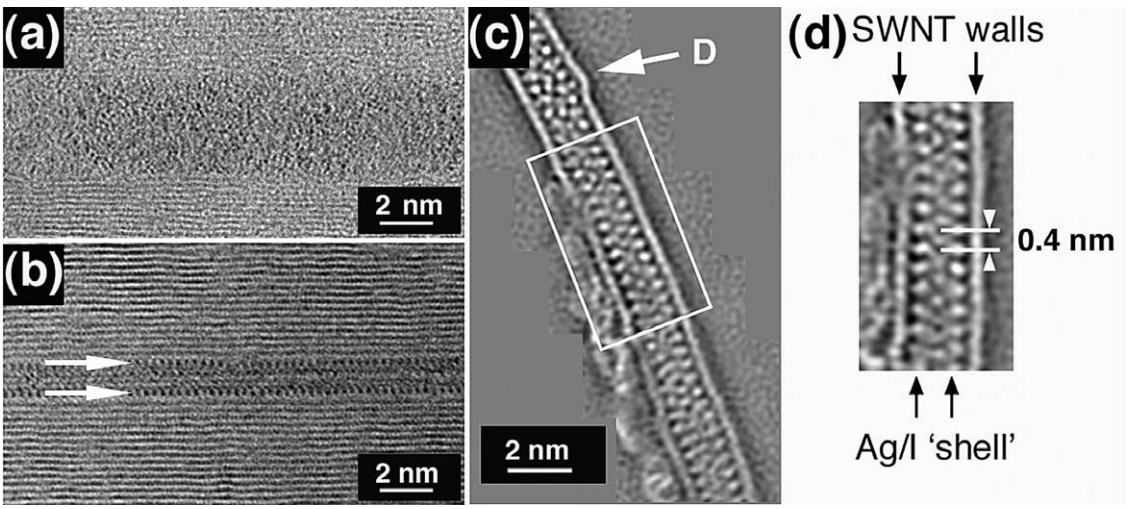

Fig. 7. (a) and (b) HRTEM images showing filling of composition B (see Fig. 5(a)) in wide (ca. 4 nm) and narrow (ca. 1 nm) diameter MWNTs respectively. Note "shell"-like microstructure formed on the walls of the nanotube. The dark spots correspond to U^{4+} ions within UCl_x polyhedra residing on the inside surface of the innermost nanotube. (c) and (d) restored phase and detail of a HRTEM through focal series obtained from a 1.4 nm diameter SWNT filled with eutectic composition from the AgI–AgCl ternary system (see Fig. 4(b)). A shell of strongly scattering Ag^+ or I^- ions is clearly visible in the indicated region. A disordered region (**D**) is visible in (c).

Fig. 6(b)) although some local variation in composition was observed. Electron micrographs showed that this mixture formed Wurzite-like 'tunnel' crystals in narrow 1.4 nm diameter SWNTs [27]. In Fig. 7 (c) and (d), we see a further example of this filling in a wider 1.6 nm diameter SWNT. The image in this instance is not a conventional HRTEM image but a restored phase image, hence the contrast reversal [8]. In the upper region of the nanotube, the microstructure of the filling is somewhat poorly defined although individual strongly scattering Ag/I columns are clearly visible. The microstructure is also apparently disrupted by the indicated defect (i.e., D in Fig. 7(c)). Along the indicated section (reproduced in Fig. 7(d)), the filling forms a shell along the walls of the capillary in which the successive 0.4 nm spaced spots, which we take to be Ag or I columns arranged in a similar fashion to those described in the reported study [37].

3.3. Crystallisation in the narrowest nanotube capillary – formation of HgI_2 *in triple walled carbon nanotubes*

In addition to studying crystals formed in SWNTs formed *via* the arc synthesis approach, we have also observed crystal formation in nanotubes formed according to a modified CVD approach which permits the formation of multi-layer carbon

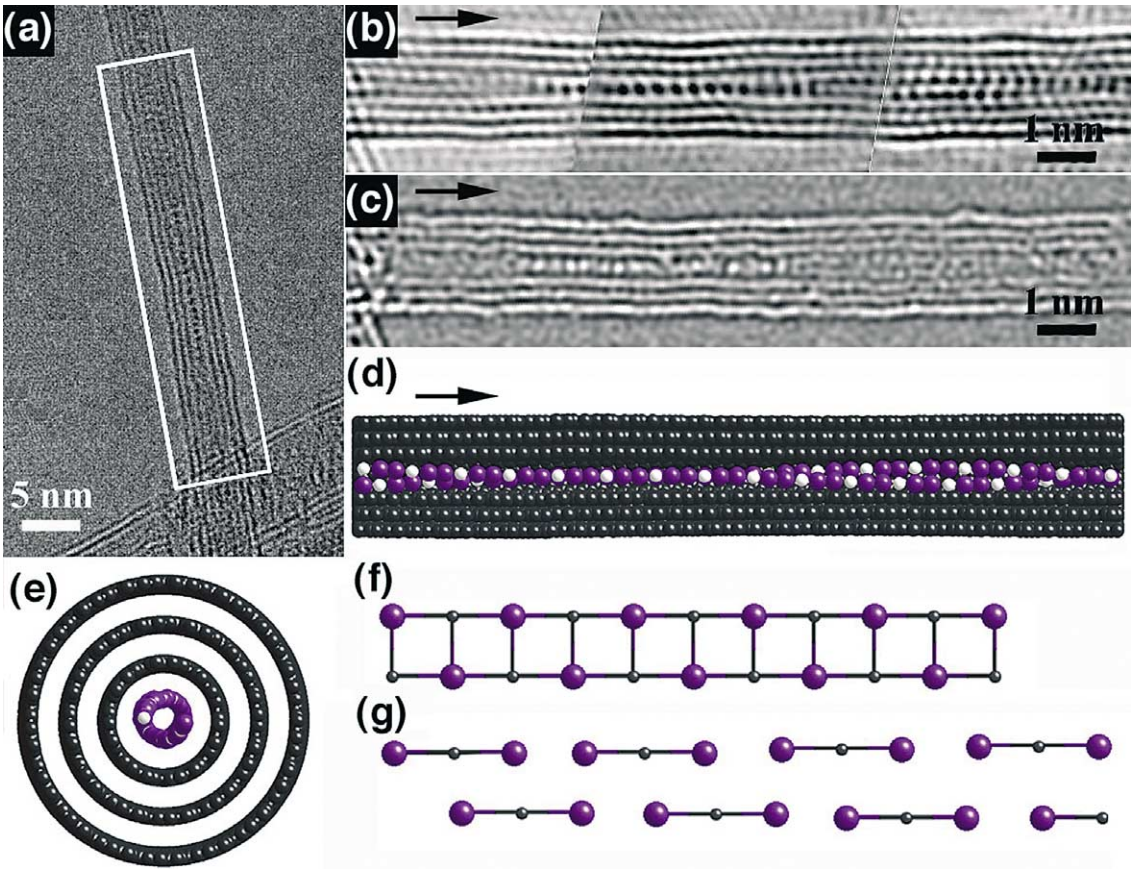

Fig. 8. (a) HRTEM image of a treble-walled carbon nanotube filled with HgI_2. (b) Composite noise-filtered image corresponding to the boxed region in (a). (b) Restored phase image produced from a 20 image through focal series of the image in (a). (d) Cutaway structural depiction of nanocomposite. (e) enlarged end-on view of (d). (f) and (g) two possible untwisted arrangements for the 2×1 crystal based on a HgI rocksalt 2×1 model and a 1D array of linear HgI_2 molecules arranged to form a 2×1 chain.

nanotubes [38]. In addition, some of these nanotubes have capillaries smaller in diameter than the typically observed SWNT diameters of 1–2 nm [23]. As a consequence, it has been possible to investigate crystal growth in even more constrained capillaries than those that we have discussed so far.

In Fig. 8(a), we can see a composite formed from a triple walled nanotube (i.e., a TWNT) and a HgI_2 1D crystal [39]. Close inspection of this crystal shows that it has a helical microstructure. In Fig. 8 (b) and (c) we show two different magnifications of the nanotube/crystal composite, one produced *via* adaptive filtering, the second *via* restoration. The helical nature of the filling may be verified by viewing these two versions along the indicating arrows in Fig. 8 (b) and (c) in a glancing direction. The HgI_2 strand can be seen as two parallel strands on the left of Fig. 8 (b) and (c) and as a single strand of doubled contrast in the left middle of the figures. To the right of this regions, the crystal bifurcates and then meets again. In addition, the diameter of the innermost nanotube is at a maximum of 0.85 nm where the crystal is visible as two layers but narrows to 0.8 nm where the crystal is visible only as one layer. We interpret this crystal to be a helically twisting $2 \times 1 \times \infty$ HgI_2 crystal, as depicted in a side-on view in Fig. 6(d) and in end-on view in Fig. 6(e).

Interpreting the microstructure of this crystal was difficult as, in the obtained image (Fig. 8(b)), there is insufficient phase contrast to distinguish the Hg^+ and I^- single atom columns unambiguously. As a result, there are several possible atom configurations for the configuration of the $2 \times 1 \times \infty$ helical chain. One possible interpretation is that it consists of a double rocksalt layer, as depicted in Fig. 8(f). This structure is unlikely as it would result in an unfavoured net stoichiometry for the 1D crystal of HgI. A second interpretation is that the crystal is derived from an assembly of HgI_2 molecules arranged as depicted in Fig. 8(g) and derived from the molecular form of this halide [40]. This interpretation is not without its problems as the HgI_2 molecules would have to be arranged in a more repulsing configuration relative to the bulk form of the halide in which the molecules are arranged in a minimum energy configuration. However, this model has the advantage that it retains the 1D crystal

in the correct stoichiometry. The only similar system to be reported was the formation of helical molecular iodine chains in ∼1.4 nm diameter SWNTs [41].

4. Conclusions

Due to their well-defined and comparatively simple atomic structures, nanotube composites may be seen as test beds for verifying theoretical concepts in the physics and materials science of low-dimensional systems. In this study, we have shown how the narrowest carbon capillaries can have a profound impact on the nanostructures of crystals formed on the smallest possible scale. These nanotube composites are extremely valuable because they can be synthesised and studied on a laboratory scale using relatively inexpensive fabrication methodologies thus making the routine study of nanoscale crystalline species with precisely regulated atomic structures entirely feasible. If the synthesis of phase pure (n, m) nanotubes ever becomes feasible, then we have the prospect to studying the bulk physical properties of crystals with precise numbers of atomic layers on a routine basis.

Acknowledgements

The authors are indebted to assistance from Miles Novotny, Robin Carter, Drs. Gareth Brown, Sam Bailey, Cigang Xu, Steffi Friedrichs, Emmanuel Flahaut, Rafal Dunin-Borkowski (now in Department Materials Science, Cambridge), Yann Astier and, in Cambridge: Drs. Rüdiger Meyer (now in the Department of Materials, Oxford) and Owen Saxton. We also indebted to Dr. Mark Wilson (now at UCL) and Prof. Paul Madden FRS of the Physical and Theoretical Laboratory, Oxford. We acknowledge financial support from the Petroleum Research Fund, administered by the ACS (Grant No. 33765-AC5) and the EPSRC (Grant Nos. GR/L59238 and GR/L22324). J.S. is indebted to the Royal Society for a University Research Fellowship.

References

[1] S. Iijima, T. Ichihashi, Nature 363 (1993) 603.
[2] D.S. Bethune, C.H. Kiang, M.S. de Vries, G. Gorman, R. Savoy, J. Vazquez, R. Beyers, Nature 363 (1993) 605.
[3] J. Sloan, A.I. Kirkland, J.L. Hutchison, M.L.H. Green, J. Chem. Soc., Chem. Commun. (2002) 1319.
[4] P.M. Ajayan, J.M. Lambert, P. Bernier, L. Barbedette, C. Colliex, J.M. Planeix, Chem. Phys. Lett. 215 (1993) 509.
[5] T. Guo, P. Nikolaev, A. Thess, D.T. Colbert, R.E. Smalley, Chem. Phys. Lett. 243 (1995) 49.
[6] P. Nikolaev, M.J. Bronikowski, R.K. Bradley, F. Rohmund, D.T. Colbert, K.A. Smith, R.E. Smalley, Chem. Phys. Lett. 313 (1999) 91.
[7] J. Sloan, M.C. Novotny, S.R. Bailey, G. Brown, C. Xu, V.C. Williams, S. Friedrichs, E. Flahaut, R.L. Callendar, A.P.E. York, K.S. Coleman, M.L.H. Green, R.E. Dunin-Borkowski, J.L. Hutchison, Chem. Phys. Lett. 329 (2000) 61.
[8] R.R. Meyer, J. Sloan, R.E. Dunin-Borkowski, A.I. Kirkland, M.C. Novotny, S.R. Bailey, J.L. Hutchison, M.L.H. Green, Science 289 (2000) 1324.
[9] J. Sloan, S.J. Grosvenor, S.R. Friedrichs, A.I. Kirkland, J.L. Hutchison, M.L.H. Green, Angew. Chem. Int. Ed. 114 (2002) 1204.
[10] C. Xu, J. Sloan, G. Brown, S.R. Bailey, V.C. Williams, S. Friedrichs, K.S. Coleman, E. Flahaut, J.L. Hutchison, R.E. Dunin-Borkowski, M.L.H. Green, J. Chem. Soc., Chem. Commun. (2000) 2427.
[11] M. Wilson, P.A. Madden, J. Am. Chem. Soc. 123 (2001) 2101.
[12] M. Wilson, J. Chem. Phys. 116 (2002) 3027.
[13] M. Wilson, Chem. Phys. Lett. 366 (2002) 504.
[14] J. Sloan, A.I. Kirkland, J.L. Hutchison, M.L.H. Green, Accts. Chem. Res. 35 (2002) 1054.
[15] S. Friedrichs, J. Sloan, M.L.H. Green, J.L. Hutchison, R.R. Meyer, A.I. Kirkland, Phys. Rev. B 64 (2001) 0454061.
[16] D.J. Hornbaker, S.-J. Kahng, S. Misra, B.W. Smith, A.T. Johnson, E.J. Mele, D.E. Luzzi, A. Yazdani, Science 295 (2002) 828.
[17] J. Lee, H. Kim, S.-J. Kahng, G. Kim, Y.-W. Son, J. Ihm, H. Kato, Z.W. Wang, T. Okazaki, H. Shinohara, Y. Kuk, Nature 415 (2002) 1005.
[18] J. Sloan, S. Friedrichs, R.R. Meyer, A.I. Kirkland, J.L. Hutchison, M.L.H. Green, Inorg. Chim. Acta 330 (2002) 1.
[19] J. Sloan, M. Terrones, S. Nufer, S. Friedrichs, S.R. Bailey, H.G. Woo, M. Rühle, J.L. Hutchison, M.L.H. Green, J. Am. Chem. Soc. 124 (2002) 2116.
[20] H. Kataura, Y. Maniwa, T. Kodama, K. Kikuchi, K. Hirahara, S. Iijima, S. Suzuki, W. Krätschmer, Y. Achiba, AIP Conf. Proc. 591 (2001) 251.
[21] B.W. Smith, R.M. Russo, S.B. Chikkannanavar, D.E. Luzzi, J. Appl. Phys. 91 (2002) 9333.
[22] G. Brown, S.R. Bailey, M. Novotny, R. Carter, E. Flahaut, K.S. Coleman, J.L. Hutchison, M.L.H. Green, J. Sloan, Appl. Phys. A 76 (2003) 1–6.
[23] C. Journet, W.K. Maser, P. Bernier, A. Loiseau, M. Lamy de la Chappelle, S. Lefrant, P. Derniard, R. Lee, J.E. Fisher, Nature 388 (1997) 756.
[24] P.M. Ajayan, S. Iijima, Nature 361 (1993) 333.

[25] J. Sloan, D.M. Wright, H.G. Woo, S. Bailey, G. Brown, A.P.E. York, K.S. Coleman, J.L. Hutchison, M.L.H. Green, J. Chem. Soc., Chem. Commun. (1999) 699.
[26] P. Cortona, Phys. Rev. B 46 (1992) 2008.
[27] R.B. Srinivasa, S.P. Sanyal, Phys. Rev. B 42 (1990) 1810.
[28] M. Ahtee, Annal. Acad. Sci. Fenn. Ser. A6 313 (1969) 1.
[29] M. Blackman, I.H. Khan, Proc. Roy. Soc. 77 (1961) 471.
[30] G. Brown, S.R. Bailey, J. Sloan, C. Xu, S. Friedrichs, E. Flahaut, K.S. Coleman, M.L.H. Green, J.L. Hutchison, R.E. Dunin-Borkowski, J. Chem. Soc., Chem. Commun. (2001) 845.
[31] A.F. Wells, Structural Inorganic Chemistry, 5th edition, Clarendon Press, 1984, p. 315.
[32] C.E. Weir, G.J. Piermarini, J. Nat. Bur. Stand. 68 (1964) 105.
[33] B.W. Smith, M. Monthioux, D.E. Luzzi, Nature 396 (1998) 323.
[34] J. Sloan, R.E. Dunin-Borkowski, J.L. Hutchison, K.S. Coleman, V.C. Williams, J.B. Claridge, A.P.E. York, C. Xu, S.R. Bailey, G. Borwn, S. Friedrichs, M.L.H. Green, Chem. Phys. Lett. 316 (2000) 191.
[35] C.E. Weir, G.J. Piermarini, J. Nat. Bur. Stand. 66 (1962) 325.
[36] J. Sloan, J. Cook, A. Chu, M. Zwiefka-Sibley, M.L.H. Green, J.L. Hutchison, J. Solid State Chem. 140 (1998) 83.
[37] J. Sloan, M. Terrones, S. Nufer, S. Friedrichs, S.R. Bailey, H.G. Woo, M. Rühle, J.L. Hutchison, M.L.H. Green, J. Am. Chem. Soc. 124 (2002) 2116.
[38] A. Peigney, P. Coquay, E. Flahaut, R.E. Vandenberghe, E. De Grave, C. Laurent, J. Phys. Chem. B 105 (2001) 9699.
[39] X. Cu, Ph.D. Thesis, Oxford, 2001, pp. 220–223..
[40] R.J. Havighurst, J. Am. Chem. Soc. 48 (1926) 2113.
[41] X. Fan, E.C. Dickey, P.C. Eklund, K.A. Williams, L. Grigorian, R. Buckzo, S.T. Pantelides, S.J. Pennycook, Phys. Rev. Lett. 84 (2000) 4621.